Virtual prototyping of non-invasive spinal cord electrical stimulation targeting upper limb motor function
Supplementary Information

Abdallah Alashqar[1,2], Nabila Brihmat[3], Vincent Gemar[1,2], Zhaoshun Hu[1,2], Seong-Ryong Koh[4], Sandra Diaz-Pier[5], Roberto de Freitas[6,7,8], Atsushi Sasaki[9], Matija Milosevic[6,10,11,12], Rodolfo Keesey[13,14], Ismael Seáñez[13,14,15,16], Esra Neufeld[17], Hélène Cassoudesalle[18], Ursula Hofstoetter[19], Karen Minassian[19], Fabien Wagner[3], Andreas Rowald[1,2]

[1] Department of Medical Informatics, Biometry and Epidemiology, Friedrich-Alexander-Universität Erlangen-Nürnberg, Erlangen 91052, Germany
[2] Department of Artificial Intelligence in Biomedical Engineering, Friedrich-Alexander-Universität Erlangen-Nürnberg, Erlangen 91052, Germany
[3] Univ. Bordeaux, CNRS, IMN, UMR 5293, F-33000 Bordeaux, France
[4] Simulation and Data Lab Highly Scalable Fluids & Solids Engineering, Jülich Supercomputing Ctr. (JSC), Institute for Advanced Simulation, Forschungszentrum Jülich GmbH, 52428 Jülich, Germany
[5] Simulation and Data Lab Neuroscience, Jülich Supercomputing Ctr. (JSC), Institute for Advanced Simulation, Forschungszentrum Jülich GmbH, 52428 Jülich, Germany
[6] Department of Mechanical Science and Bioengineering, Graduate School of Engineering Science, Osaka University, Toyonaka, Japan
[7] Rehab Neural Engineering Labs, University of Pittsburgh, Pittsburgh, PA 15219, USA
[8] Department of Neurological Surgery, University of Pittsburgh, Pittsburgh, PA 15260, USA
[9] Department of Life Sciences, Graduate School of Arts and Sciences, The University of Tokyo, Meguro-ku, Tokyo 153-8902, Japan
[10] The Miami Project to Cure Paralysis, Miller School of Medicine, University of Miami, Miami, FL 33136, USA
[11] Department of Neurological Surgery, Miller School of Medicine, University of Miami, Miami, FL 33136, USA
[12] Department of Biomedical Engineering, University of Miami, FL 33146, USA
[13] Department of Biomedical Engineering, Washington University in St. Louis, St. Louis, MO 63105, USA
[14] Division of Neurotechnology, School of Medicine, Washington University in St. Louis, MO 63110, USA
[15] Department of Neurosurgery, School of Medicine, Washington University in St. Louis, MO 63110, USA
[16] Preston M. Green Department of Electrical and Systems Engineering, Washington University in St. Louis, MO 63130, USA
[17] Foundation for Research on Information Technologies in Society (IT'IS), Zürich 8004, Switzerland
[18] Department of Physical Medicine and Rehabilitation, CHU de Bordeaux, F-33000 Bordeaux, France
[19] Center for Medical Physics and Biomedical Engineering, Medical University of Vienna, Vienna 1090, Austria

Corresponding author:
Andreas Rowald, PhD
Friedrich-Alexander-Universität Erlangen-Nürnberg
andreas.rowald@fau.de

Supplementary methods:

End-nodal recruitment:

We noticed a phenomenon of end-nodal recruitment for some axons, a known limitation of conductance-based compartmental cable models[3,4]. To ensure the interpretability of our simulation results, we sought to avoid such activations. Therefore, we introduced two methods of avoiding phantom end-node activations and assessed their ability in shifting the initiation sited of action potentials (ISAPs), in addition to their effect on the threshold of activation (**Supplementary Fig. 1**). Based on our results, we replaced terminal nodes with passive nodes to avoid end-node recruitment[3] (**Supplementary Fig. 1**).

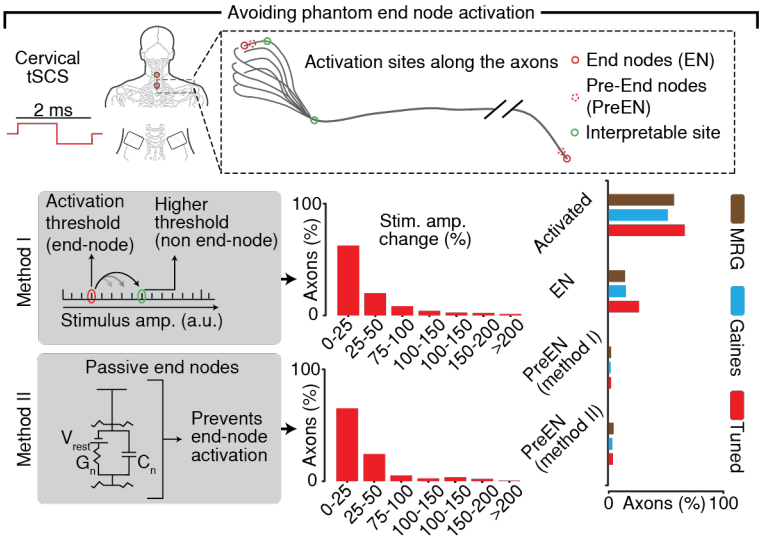

Supplementary Fig. 1. Proposed methods for avoiding non-interpretable end-node activations observed in simulations of extracellularly stimulating conductance-based compartmental cable models[3,4]. Top: electrode configuration where end-nodes activations could occur and end-nodes highlighted along a sketch of nerve axons. Bottom: Proposed methods for avoiding phantom end-node activations. Method I: Avoiding end-node activation by increasing stimulus amplitude until a new activation site is present. Method II: Avoiding end-node activation by replacing the nodes of Ranvier at the termini with passive nodes[3], preventing any activation to be initiated from them. The red bar plots show histograms of the relative stimulus threshold changes caused by using each of the methods on the tuned cable model, while the vertical bar chart shows the percentage of axons exhibiting end-node activation as well as the percentage of axons where the activation moved to only the next node after applying each of the two methods using each of the three different cable models. Abbreviations: millisecond (ms), end nodes (EN), pre-end nodes (PreEN), nodal conductance (G_n), nodal capacitance (C_n), resting membrane potential (V_{rest}).

Axon model tuning:

As mentioned in the methods' subsection "Axon model tuning", we constructed a parameter space composed of all parameters, for which we found reported variations[5–14] of ion channel properties between somatosensory afferents and motor efferents (**Supplementary Table 4**). We ensured that all sampled parameter combinations preserved the reported property differences[5–14] (**Supplementary Table 4**).

Supplementary tables:

Segment	Reported avg. segment length[1] (mm)	Reported avg. REZ length[1] (mm)	Reported avg. segment length percentage[2] (%)	Calculated segment length (mm)	Calculated ratio (avg. REZ length / avg. segment length)	Calculated REZ length (mm)
C1	12.60*	11.30*	1.60	7.57	0.90	6.79
C2	12.60	11.30	2.20	10.41	0.90	9.34
C3	13.30	9.40	3.50	16.57	0.71	11.71
C4	13.90	11.60	3.50	16.57	0.83	13.83
C5	15.00	12.40	3.50	16.57	0.83	13.70
C6	13.60	11.50	3.30	15.62	0.85	13.21
C7	11.70	11.40	3.20	15.15	0.97	14.76
C8	12.50	11.80	3.40	16.09	0.94	15.19
T1	13.00	12.00	3.60	17.04	0.92	15.73
T2	16.40	13.10	3.90	18.46	0.80	14.75
T3	16.10	15.30	4.40	20.83	0.95	19.79
T4	22.80	18.40	5.00	23.67	0.81	19.10
T5	22.10	19.60	5.10	24.14	0.89	21.41
T6	24.80	18.80	5.60	26.51	0.76	20.09
T7	24.50	20.10	5.60	26.51	0.82	21.75
T8	25.50	19.00	5.40	25.56	0.75	19.04
T9	23.90	20.40	5.10	24.14	0.85	20.60
T10	25.30	19.30	4.70	22.25	0.76	16.97
T11	22.40	15.50	4.30	20.35	0.69	14.08
T12	18.40	15.60	3.90	18.46	0.85	15.65
L1	17.50	15.20	3.60	17.04	0.87	14.80
L2	14.00	11.80	2.80	13.25	0.84	11.17
L3	11.20	11.20	2.40	11.36	1.00	11.36
L4	12.50	11.60	2.20	10.41	0.93	9.66
L5	9.70	11.20	1.70	8.05	1.15	9.29
S1	9.70*	11.20*	1.50	7.10	1.15	8.20
S2	9.70*	11.20*	1.60	7.57	1.15	8.74
S3	9.70*	11.20*	1.40	6.63	1.15	7.65
S4	9.70*	11.20*	1.30	6.15	1.15	7.10

Supplementary Table 1. Reported[1] and calculated segment-specific morphometric parameters used for the 3D rootlets model generation. *These parameters were not reported in the referenced publication but were extrapolated from parameters of the closest reported segments. Abbreviations: average (avg.), millimeter (mm), root entry zone (REZ).

Segment	Reported avg. number of rootlets[1]		Calculated number of rootlets		Reported avg. root diameter[1] (mm)		Calculated rootlet diameter (mm)	
	P	A	P	A	P	A	P	A
C1	8.33*	8.33*	5	5	4.34*	2.79*	0.87	0.56
C2	8.33	8.33	7	7	4.34	2.79	0.62	0.40
C3	8.25	6.25	11	8	4.55	2.63	0.41	0.33
C4	8.87	7.62	11	9	4.84	2.85	0.44	0.32
C5	9.22	8.14	10	9	5.43	3.78	0.54	0.42
C6	8.77	6.85	10	8	5.08	3.29	0.51	0.41
C7	7.77	7.25	10	9	5.50	2.92	0.55	0.32
C8	7.66	6.62	10	9	5.18	2.19	0.52	0.24
T1	6.00	4.66	8	6	3.85	1.80	0.48	0.30
T2	5.00	4.33	6	5	3.35	1.82	0.56	0.36
T3	4.88	4.22	6	6	3.37	1.33	0.56	0.22
T4	4.44	4.33	5	4	3.21	1.38	0.64	0.34
T5	4.00	4.88	4	5	3.29	1.47	0.82	0.29
T6	4.55	4.44	5	5	3.62	1.71	0.72	0.34
T7	4.22	4.66	5	5	3.27	1.71	0.65	0.34
T8	4.55	4.66	5	5	3.73	1.64	0.75	0.33
T9	5.44	4.66	6	5	3.83	1.43	0.64	0.29
T10	4.88	4.55	4	4	3.71	1.67	0.93	0.42
T11	5.33	3.88	5	4	3.20	1.32	0.64	0.33
T12	6.22	4.11	6	4	3.53	1.47	0.59	0.37
L1	7.22	5.33	7	5	3.84	2.45	0.55	0.49
L2	8.00	5.88	8	6	4.60	2.94	0.57	0.49
L3	8.55	6.33	8	6	4.26	2.70	0.53	0.45
L4	7.55	5.00	6	4	4.40	3.19	0.73	0.80
L5	8.22	5.33	7	5	4.98	2.83	0.71	0.57
S1	8.22*	5.33*	6	4	4.98*	2.83*	0.83	0.71
S2	8.22*	5.33*	7	4	4.98*	2.83*	0.71	0.71
S3	8.22*	5.33*	5	3	4.98*	2.83*	1.00	0.94
S4	8.22*	5.33*	5	3	4.98*	2.83*	1.00	0.94

Supplementary Table 2. Reported[1] and calculated segment- and position-specific morphometric parameters used for the 3D rootlets model generation. *These parameters were not reported in the referenced publication but were extrapolated from parameters of the closest reported segments. Abbreviations: average (avg.), millimeter (mm), posterior (P), anterior (A)

Root pairs	Left		Right	
	Reported occurrences[1] (n=9)	**Modelled**	**Reported occurrences**[1] (n=9)	**Modelled**
C2-C3	7	✓	4	X
C3-C4	9	✓	6	✓
C4-C5	6	✓	4	X
C5-C6	7	✓	7	✓
C6-C7	7	✓	5	✓
C7-C8	6	✓	5	✓
C8-T1	2	X	2	X
L1-L2	2	X	1	X
L2-L3	0	X	0	X
L3-L4	2	X	1	X
L4-L5	1	X	0	X
L-S1	1	X	0	X

Supplementary Table 3. Reported occurrences of inter-root anastomoses[1] and their inclusion in the modeling of the 3D structures in our model. Only anastomoses with occurrences 5 or more occurrences (>50%) were considered in the modeling.

Tissue	Maximum step (X, Y, Z in mm)	Geometry resolution (X, Y, Z in mm)
Rootlets	0.22, 0.22, 0.22	0.18, 0.18, 0.18
Peripheral nerves	2.0, 2.0, 2.0	1.0, 1.0, 1.0
Cranial nerve branches (including vagus nerve)	2.0, 2.0, 2.0	1.45, 1.45, 1.45
Gray matter, white matter (SC), cerebrospinal fluid and dura mater	1.0, 1.0, 2.0	1.0, 1.0, 1.0
Skin	0.5, 0.5, 1.0	0.5, 0.5, 1.0
Tissue hole filler	3.0, 3.0, 5.0	3.0, 3.0, 10.0
Other tissues	2.0, 2.0, 10.0	2.0, 2.0, 2.0

Supplementary Table 4. Voxelization parameters used for the different tissues in the 3D whole-body model. Abbreviations: millimeter (mm), spinal cord (SC).

Ion channel property	Sensory / motor difference
Persistent sodium conductance (gNa_p)	Sensory > motor[5–7]
Slow potassium conductance (gK_s)	Sensory > motor (ratio = 1.55)[8,9]
Fast potassium conductance (gK_f)	Sensory < motor (ratio = 0.6)[10]
Leakage conductance (gL)	Sensory > motor (ratio = 1.5)[11]
Persistent sodium speed (αm_pA, βm_pA)	Sensory < motor[12]
Fast sodium speed (αmA, βmA)	Sensory < motor[12]
Sodium inactivation speed (αhA, βhA)	Sensory > motor[8,12]
Slow potassium speed (αsA, βsA)	Sensory > motor[13]
Slow potassium half-activation voltage (αsB, βsB)	Sensory < motor[10,14]
Fast potassium speed (αnA, βnA)	Sensory > motor[13]

Supplementary Table 5. Ion channel differences between sensory and motor nerve fibers as reported in the literature across different species. α parameters refer to opening of ion channels, while β parameters refer to closing of ion channels.

	Node			FLUT			MYSA, STIN
Voltage and time dependent parameters	A(ms^{-1})	B(mV)	C(mV)	A(ms^{-1})	B(mV)	C(mV)	
αm	1.86	21.4	10.3	–	–	–	-
βm	0.086	25.7	9.16	–	–	–	-
αmp	0.01	27	10.2	–	–	–	-
βmp	0.00025	34	10	–	–	–	-
αh	**0.0728**	114.0	11.0	–	–	–	-
βh	2.3	31.8	13.4	–	–	–	–
αn	-	-	-	0.0462	-83.2	1.1	-
βn	-	-	-	0.0824	**-60.8684**	10.5	-
αs	0.3	-27**	-5	-	-	-	-
βs	**0.048**	10	-1	-	-	-	-
Channel Conductances	(mS cm-2)			(mS cm-2)			(mS cm-2)
Persistent Sodium	10			–			-
Fast Sodium	3000			–			-
Slow Potassium	80			-			-
Fast Potassium	-			20			-
Leak	7			-			-
Passive	-			0.1*			1 (MYSA), 0.1 (STIN)*
Reversal Potentials	(mV)			(mV)			
Sodium	50			–			-
Slow Potassium	-90.0			-			-
Fast Potassium	-			-90.0			-
Leak	-90.0			-			-
Resting potential (mV)	-78.05						

Supplementary Table 6. Parameters used in the newly-tuned MRG-type model for somatosensory afferent axons. Highlighted are values that deviated from those reported in the original MRG-model[8]. *This parameter scales with the ratio of segment diameter to fiber diameter as in the original MRG-model[8]. **To avoid spontaneous activation, this parameter was modified for very small fibers (diameter < 5.16μm) but maintained sensory/motor difference (23 mV). Abbreviations: fluted (FLUT), stereotyped Internode (STIN), myelin sheath attachment (MYSA), ion channel conductance (g), ion channel opening rate (α), ion channel closing rate (β), ion channel maximum speed of transition (A), ion channel half-activation voltage (B), ion channel response slope (C), sodium activation (m), persistent sodium activation (mp), sodium inactivation (h), fast potassium activation (n), slow potassium activation (s), millisecond (ms), millivolt (mV), milli Siemens (mS), centimeter (cm)

	Node			FLUT			MYSA, STIN
Voltage and time dependent parameters	A(ms^{-1})	B(mV)	C(mV)	A(ms^{-1})	B(mV)	C(mV)	
αm	**1.95789**	21.4	10.3	–	–	–	-
βm	**0.090526**	25.7	9.16	–	–	–	-
αmp	**0.016**	27	10.2	–	–	–	-
βmp	**0.00036959**	34	10	–	–	–	-
αh	**0.0728**	114.0	11.0	–	–	–	-
βh	**2.1789**	31.8	13.4	–	–	–	–
αn	-	-	-	**0.037149**	-83.2	1.1	-
βn	-	-	-	**0.0515**	-66	10.5	-
αs	0.3	-27	-5	-	-	-	-
βs	0.03	10	-1	-	-	-	-
Channel Conductances	(mS cm-2)			(mS cm-2)			(mS cm-2)
Persistent Sodium	10			–			-
Fast Sodium	3000			–			-
Slow Potassium	80			-			-
Fast Potassium	-			20			-
Leak	7			-			-
Passive	-			0.1*			1 (MYSA), 0.1 (STIN)*
Reversal Potentials	(mV)			(mV)			
Sodium	50			–			-
Slow Potassium	-90.0			-			-
Fast Potassium	-			-90.0			-
Leak	-90.0			-			-
Resting potential (mV)	-79.5						

Supplementary Table 7. Parameters used in the tuned MRG-type model for motor efferent axons[8]. Highlighted are values that deviated from those reported in the original MRG-model. *This parameter scales with the ratio of node diameter to fiber diameter as in the original MRG-model[8]. Abbreviations: fluted (FLUT), stereotyped Internode (STIN), myelin sheath attachment (MYSA), ion channel conductance (g), ion channel opening rate (α), ion channel closing rate (β), ion channel maximum speed of transition (A), ion channel half-activation voltage (B), ion channel response slope (C), sodium activation (m), persistent sodium activation (mp), sodium inactivation (h), fast potassium activation (n), slow potassium activation (s), millisecond (ms), millivolt (mV), milli Siemens (mS), centimeter (cm)

References

1. Mendez, A. *et al.* Segment-Specific Orientation of the Dorsal and Ventral Roots for Precise Therapeutic Targeting of Human Spinal Cord. *Mayo Clin. Proc.* **96**, 1426–1437 (2021).
2. Frostell, A., Hakim, R., Thelin, E. P., Mattsson, P. & Svensson, M. A Review of the Segmental Diameter of the Healthy Human Spinal Cord. *Front. Neurol.* **7**, (2016).
3. Golabek, J., Schiefer, M., Wong, J. K., Saxena, S. & Patrick, E. Artificial neural network-based rapid predictor of biological nerve fiber activation for DBS applications. *J. Neural Eng.* **20**, 016001 (2023).
4. Rubinstein, J. T. Axon termination conditions for electrical stimulation. *IEEE Trans. Biomed. Eng.* **40**, 654–663 (1993).
5. Mogyoros, I., Kiernan, M. C. & Burke, D. Strength-duration properties of human peripheral nerve. *Brain* **119**, 439–447 (1996).
6. Bostock, H. & Rothwell, J. C. Latent addition in motor and sensory fibres of human peripheral nerve. *J. Physiol.* **498**, 277–294 (1997).
7. Mogyoros, I. Excitability changes in human sensory and motor axons during hyperventilation and ischaemia. *Brain* **120**, 317–325 (1997).
8. McIntyre, C. C., Richardson, A. G. & Grill, W. M. Modeling the Excitability of Mammalian Nerve Fibers: Influence of Afterpotentials on the Recovery Cycle. *J. Neurophysiol.* **87**, 995–1006 (2002).
9. Neumcke, B., Schwarz, W. & Stämpfli, R. Differences between K channels in motor and sensory nerve fibres of the frog as revealed by fluctuation analysis. *Pflüg. Arch.* **387**, 9–16 (1980).
10. Dubois, J. M. Potassium currents in the frog node of Ranvier. *Prog. Biophys. Mol. Biol.* **42**, 1–20 (1983).
11. Neumcke, B. & Stämpfli, R. Sodium currents and sodium-current fluctuations in rat myelinated nerve fibres. *J. Physiol.* **329**, 163–184 (1982).
12. Mitrović, N., Quasthoff, S. & Grafe, P. Sodium channel inactivation kinetics of rat sensory and motor nerve fibres and their modulation by glutathione. *Pflüg. Arch.* **425**, 453–461 (1993).
13. Palti, Y., Moran, N. & Stämpfli, R. Potassium currents and conductance. Comparison between motor and sensory myelinated fibers. *Biophys. J.* **32**, 955–966 (1980).
14. Bretag, A. H. & Stämpfli, R. Differences in action potentials and accommodation of sensory and motor myelinated nerve fibres as computed on the basis of voltage clamp data. *Pflüg. Arch.* **354**, 257–271 (1975).